TRENDS IN SCIENCES 2026; 23(2): 11365
https://doi.org/10.48048/tis.2026.11365 RESEARCH ARTICLE

Fabrication and Exploring the Features of (Organic Polymer-Graphene Oxide) New Nanostructures for Nanoelectronics and Biomedical Applications

Saja Mohammed Hussein Ali[1], Bahaa H. Rabee[1], Najah M. L. Al Maimuri[2] and Ahmed Hashim[1,*]

[1]Department of Physics, College of Education for Pure Sciences, University of Babylon, Babylon 51001, Iraq
[2]Building and Construction Technologies Engineering Department, College of Engineering and Engineering Technologies, Al-Mustaqbal University, Babylon 51001, Iraq

([*]Corresponding author's e-mail: ahmed_taay@yahoo.com)

Received: 24 July 2025, Revised: 18 August 2025, Accepted: 25 August 2025, Published: 10 November 2025

Abstract

This work aims to fabricate of PVA-GO new bionanocomposites films. The effect GO NPs on structural, morphological, optical features of PVA was investigated. The XRD and FTIR patterns demonstrated the presence of suitable peaks and shifts for the prepared composite material. These nanocomposites were then used to prepare artificial leather. The series of PVA/GO hydrogels with a fixed PVA ratio and varying the GO content at 0.1, 0.05, 0.025, and 0.012 wt% were prepared. We used a multiple freeze-thaw method to ensure the formation of a homogeneous porous structure, followed by ultrasonic treatments to disperse and distribute the GO within the polymer matrix. Samples were cured before and after cutting at room temperature, and the self-healing rate was measured through tests and monitoring the time course of shear strength and bond density. The preparation process focused on selecting the appropriate nanomaterial concentration to match the quality of the prepared leather in terms of durability, elasticity, and self-healing or repairing rate. This was done using ultraviolet-visible (UV-Vis), Fourier transform infrared (FTIR), optical microscopy, and atomic force microscopy (AFM). The results showed that a concentration of 0.05% was the most suitable for preparation. This study represents a careful attempt to determine the optimal break-even point between the amount of GO available to build sufficient dynamic bonds and the ease of movement of the PVA chains; the optimal ratio provided the highest healing rate.

Keywords: Graphene, Nanooxide, Nanostructures, Thin films, Graphite, Optical properties

Introduction

In the last 2 decades, graphene oxide (GO) has topped the list of the most researched 2-dimensional materials due to its unique combination of a large specific surface area and a variety of functional groups (hydroxyl, epoxide, carboxyl), giving it an exceptional ability to interact with polymer matrices and modify their mechanical and electrical properties [1]. GO is prepared using the conventional modified Hummers method, in which graphite is oxidized with a mixture of concentrated sulfuric acid and potassium permanganate under carefully controlled temperature and addition rates, followed by washing and ultrasonic shock to separate nanosheets and trap oxygen groups on the surface. Critical reviews have shown that controlling the degree of oxidation and particle size of the graphite introduced into the process is key to adjusting the density of functional groups and the homogeneity of sheet distribution, enabling smooth integration of GO into polymeric networks without forming agglomerates that reduce the effectiveness of dynamic bonding [2]. Subsequent studies have demonstrated the adaptability of Hummers' method by using environmental accelerators such as hydrogen peroxide or reducing the acid washing steps, thus mitigating the environmental

impact and enhancing the material's yield without compromising its purity or the abundance of its functional groups [3].

The importance of GO in the field of smart artificial skin manufacturing stems from its ability to enhance the self-healing and sensory function of the composite [4]. In the hydrogel structures used as the basis for this type of artificial skin, GO sheets act as multi-connecting sites that create an interconnected network that increases the tensile and stretching resistance, while simultaneously enabling the rapid rebuilding of hydrogen and electrostatic bonds after the structure is torn or scratched [5]. A recent review of electronic skin interfaces showed that incorporating GO into flexible polymer matrices provides the material with a wide sensing range in response to pressure and stretching, with a recovery efficiency exceeding 80% of its original properties within a few minutes, without the need for chemical stimuli or external energy. The work published in ScienceDirect also demonstrated that hydrogels embedded with GO strips show promising potential for tissue engineering and regenerative medicine applications, providing a supportive network that adapts to cellular growth and spontaneously restructures after mechanical damage without causing toxicity to the surrounding environment or biological tissues [6].

The combination of high-quality GO preparation and controlled distribution within flexible hydrogels forms the basis for developing artificial skins capable of mimicking the biological performance of skin, achieving a delicate balance between durability, elasticity, and self-healing ability [7-11]. There are different types of graphene oxide synthesis methods [12,13]. The nanocomposites were fabricated to employ in various applications [14,15]. This work aims to fabricate of PVA-GO new bionanocomposites films. The effect GO NPs on structural, morphological, optical features of PVA was investigated. The PVA-GO fabricated bionanocomposites may be utilized in a variety of biological and nanoelectronics applications. The research will also examine the relationship between GO concentration and healing efficiency, using FTIR spectroscopy to analyze the nature of the bonds, SEM and OM techniques to assess morphological distribution, and capacitive tensile tests and electrical conductivity measurements before and after healing to assess functional performance.

Materials and methods

Graphite rods were used with concentrated sulfuric acid (HCl) 98% as well as sodium nitrate (Na_2NO_3) 97% and potassium permanganate ($KMNO_4$) 99.5% with hydrogen peroxide (H2O2) 80% extra pure, and Poly(vinyl alcohol) 99%.

Preparation of nano-graphene oxide

Graphene oxide nanoparticles were prepared by adding 23 mL of concentrated sulfuric acid to a 1000 mL beaker placed in an ice bath. Zero point five g of graphite powder was then slowly added to the acid solution for 10 min. 0.025 g of sodium nitrate was then added to the mixture for 15 min. After an hour, 1.5 g of potassium permanganate was added very slowly [16,17]. The mixture was then left on a magnetic stirrer for 24 h at 35 °C. 250 mL of distilled water was added to the mixture and left for 1 h to homogenize the solution. 32% hydrogen peroxide was then added to remove any remaining potassium permanganate [18,19]. The mixture was left to cool for half an hour, and then the product was washed with sulfuric acid and deionized water [20,21]. It was stored overnight in a desiccator that contains a silica gel. As shown in **Figure 1**.

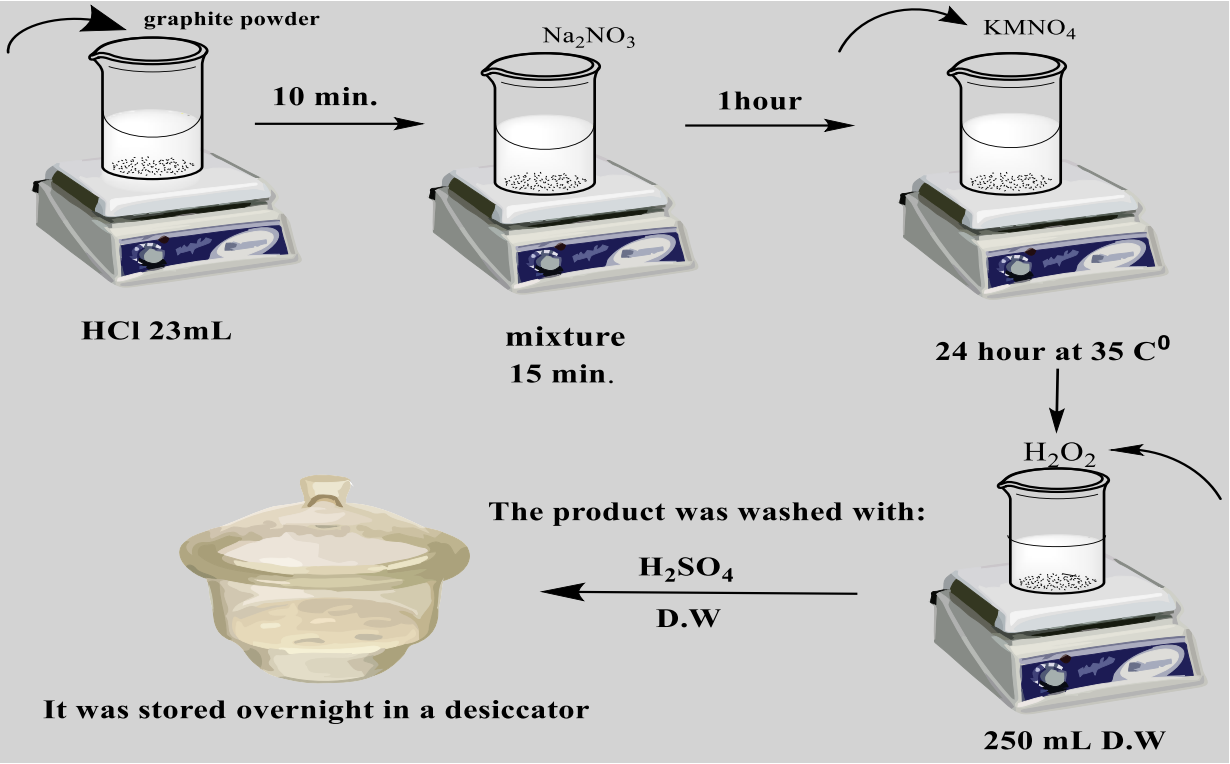

Figure 1 The schematic diagram for the synthesis process of the of nano-graphene oxide.

Artificial leather preparation method

To create the artificial leather, polyvinyl alcohol was dissolved in an aqueous solution at 90 °C for 1 h. Various concentrations of Nano graphene oxide were then added, at ratios of 1:1, 1:2, 1:3, and 1:4, to the nano graphene oxide solution. The mixture was left on a magnetic stirrer for 1 h to homogenize. Crosslinking agents, including 0.3 g of sodium borate and 0.3 g of acetic acid, were then added. Five mL of glycerol was then added to increase elasticity [20,21]. The mixture was then left on a magnetic stirrer for half an hour, and the hydrogel was poured into dishes as shown in **Figure 2**.

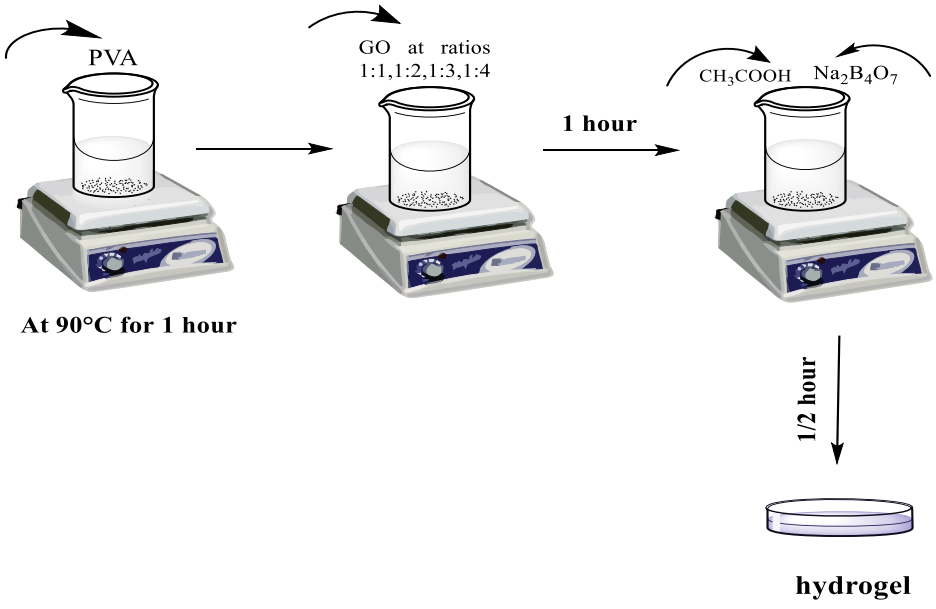

Figure 2 The schematic diagram for the synthesis process of artificial leather.

Self-healing test of synthetic leather

The self-healing test of synthetic leather was conducted at room temperature (25 °C) by making an incision in the selected sample using a sharp scalpel blade. The repair process was monitored visually and by using an Optical microscopy and atomic force microscope to observe the healing process. The time it took for the sample to fully heal (disappear the incision) was recorded [22,23].

Results and discussion

Morphology of surfaces

The prepared nanostructure was measured using a scanning electron microscope (SEM) as showed in **Figure 3**, which displays structures resembling wrinkled sheets or folded sheets, as well as an uneven surface and clear wrinkles, which is a natural feature of graphene oxide. The images showed that the preparation maintained relatively large sheet sizes, and the presence of overlapping sheets and wrinkles indicates the success of the oxidation and partial drawing process. It also indicates a local thickness or the size of small in **Figure 3(b)**, clustered flakes, which indicates the presence of a clear nanostructure [24].

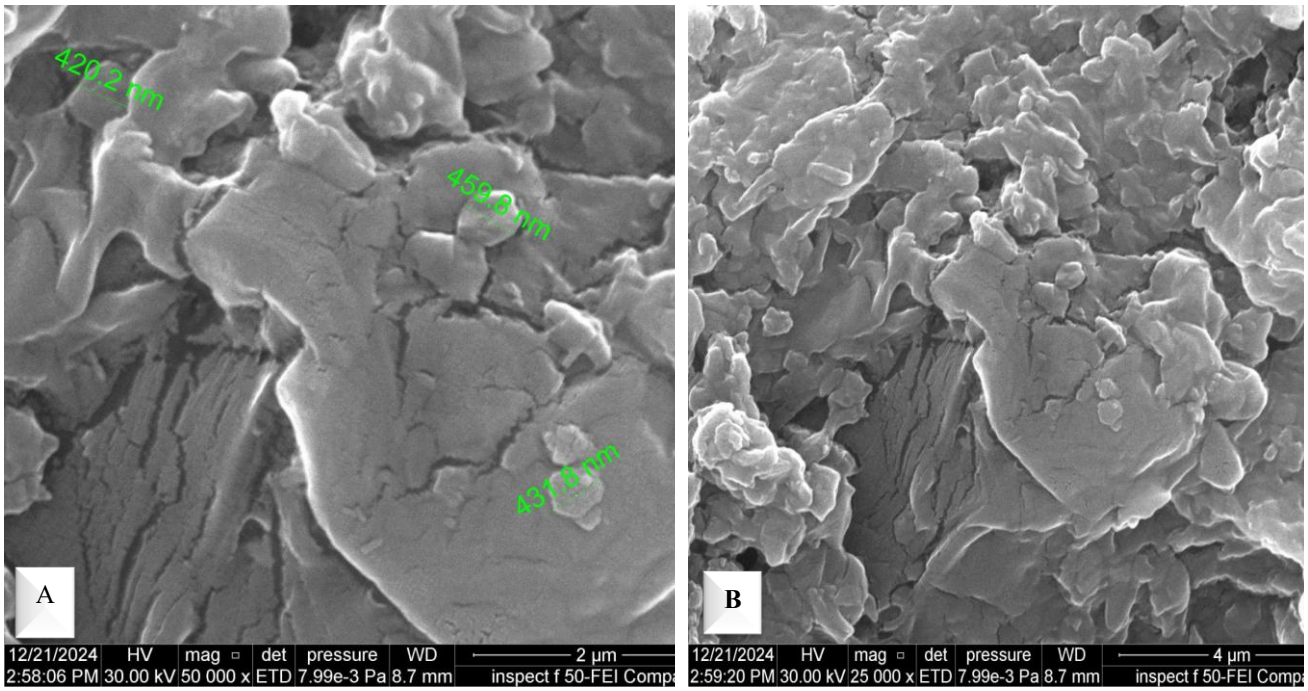

Figure 3 Prepared nanostructure and nano size.

FTIR spectrum

The structural properties of the nanomaterial were measured by FTIR as represented in **Figure 4**. We observe a broad O-H band (~3200 - 3600 cm^{-1}), graphite shows almost no absorption in this band because graphite contains no free hydroxyl groups [25]. Nano-GO, on the other hand, exhibits a broad band around 3300 cm^{-1} due to the stretching vibrations of the -OH (hydroxyl) and -COOH (carboxyl) groups, indicating the presence of bound water and hydroxyls on the oxide surface [26]. We observe a carbonyl C=O peak (~1700 - 1720 cm^{-1}), Graphite does not exhibit a clear peak here. Nano-GO, on the other hand, exhibits a strong peak at ~1698 cm^{-1}, indicating the stretching vibrations of the carbonyl group (-C=O) in a carboxylic acid or aldehyde, confirming the oxidation of the graphene structure. Epoxide C-O-C vibrations (~1220 cm^{-1}) Graphite exhibits no absorption at this location. Nano-GO exhibits a peak at ~1220 cm^{-1} due to C-O-C vibrations (epoxide bridges) in the graphene oxide structure [27]. Alcoholic C-O vibrations are also present (~1050 - 1100 cm^{-1}). Graphite exhibits no clear

peak, Nano-GO exhibits absorption at ~1050 cm^{-1} due to C-O vibrations in alkoxyl groups (C-O-H). C-H bands and other elements (<900 cm^{-1}) Both samples exhibited faint peaks at 800 - 900 cm^{-1} due to out-of-plane C-H vibrations in some impurities or interference with the device spectrum [28]. Since graphite is the pure crystalline form of carbon and does not contain oxygen functional groups, its spectrum is almost flat without functional peaks. Since the 2nd spectrum is rich in oxygen peaks of -C-O-H-, -C-O-C-, -C=O, OH groups, which confirms the success of the graphite oxidation process and its conversion to nano-graphene oxide [1,29].

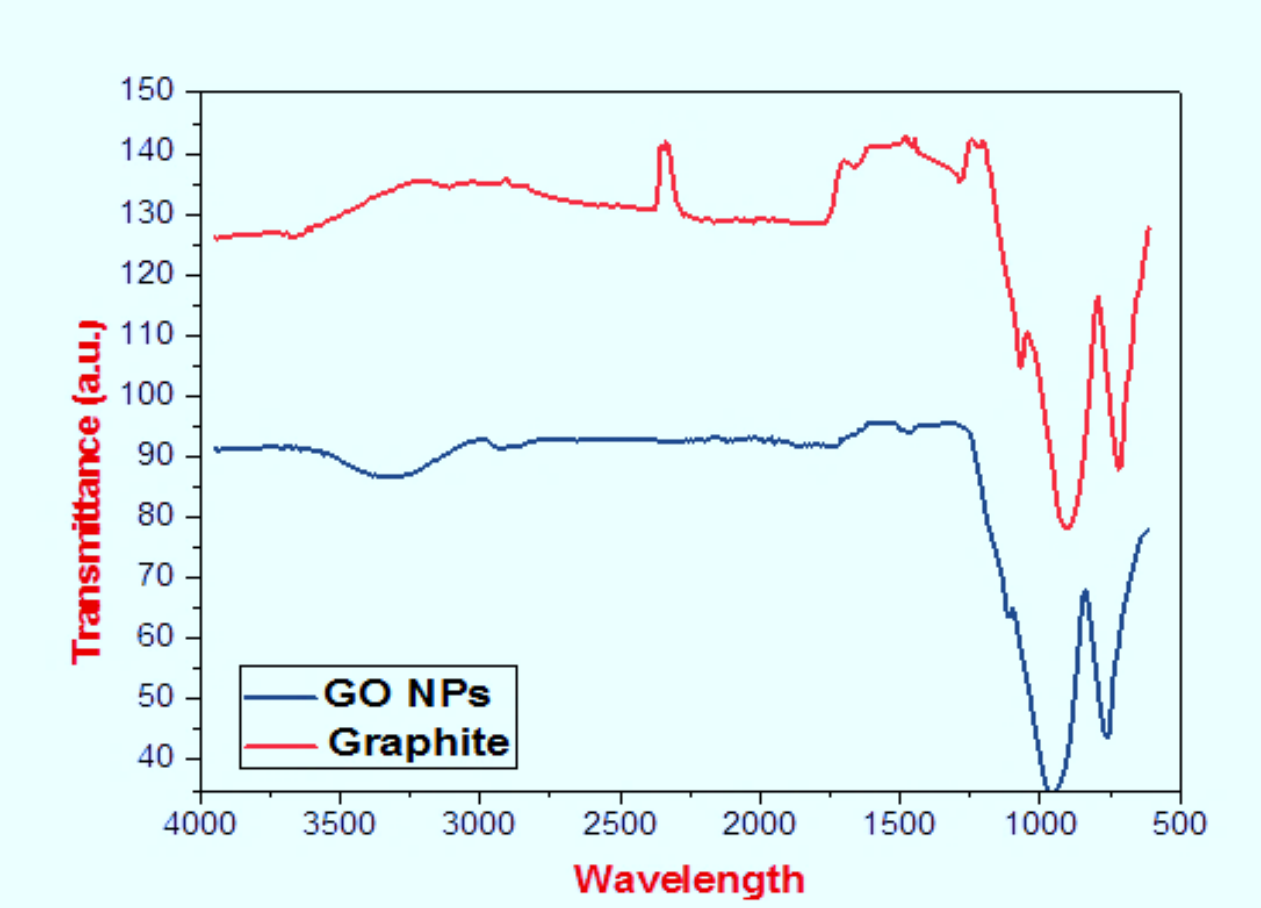

Figure 4 FTIR for (A) Graphite and (B) Nano-GO.

Figure 5 shows the FTIR spectra for PVA-nano graphene oxide nanostructures. The black (pure) spectrum is the spectrum of pure PVA, showing distinct peaks such as: OH stretching (at ~3300 cm^{-1}), CH stretching (at ~2900 cm^{-1}), C=O or C-O stretching (at ~1730 and ~1240 cm^{-1}), and C-O-C or C-C vibrations (at ~1090 - 1000 cm^{-1}). Upon the addition of graphene oxide (GO), clear changes appear in the position and intensity of some peaks, indicating an interaction between the GO functional groups (such as OH, COOH, C=O) and the PVA groups. Changes in the bonds may occur [1,30,31]. The disappearance or splitting of some peaks indicates a modification in the structural composition of the compound. Depending on the concentration, when the GO concentration increases from 0.025% to 0.12%, some peaks tend to shift or increase in intensity. The peak around 3300 cm^{-1} (OH stretching) becomes wider or moves, indicating a change in hydrogen bonding. Peaks in the 1000 - 1500 cm^{-1} region exhibit new overlaps, indicating the presence of graphene oxide. We conclude that the FTIR spectrum confirms the successful incorporation of nano-graphene oxide into the PVA matrix. At 0.025 and 0.05% GO, clear changes are evident compared to pure PVA [32]. The main peaks shift or change in intensity (especially around 3300, 1700, and 1000 cm^{-1}). Good interaction is observed without significant spectrum distortion. We

conclude that the optimum concentration of nano-graphene oxide is between 0.025% and 0.05% by weight. 0.05% by weight is likely to be preferable because it shows a clear interaction with PVA and does not cause significant spectrum distortion [33,34]. It also retains the basic chemical structure of PVA while enhancing its properties. Therefore, it was chosen for the self-healing test.

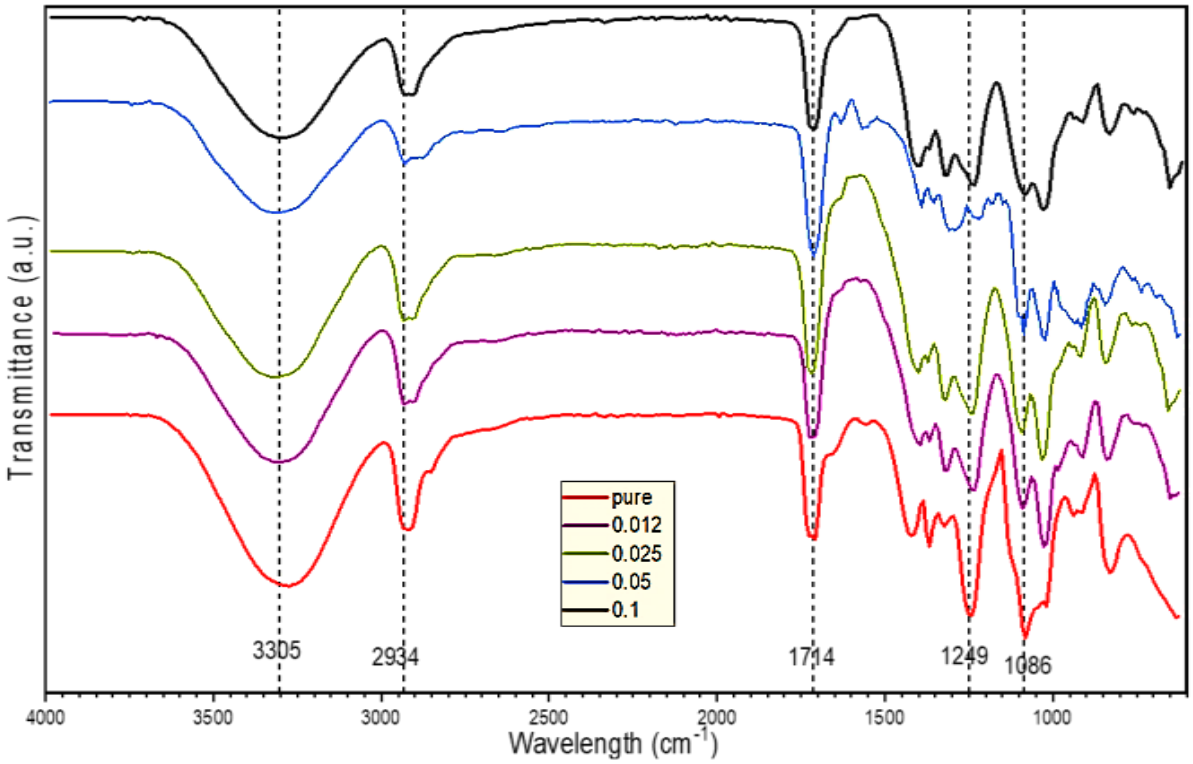

Figure 5 FTIR spectra for PVA-nano graphene oxide nanostructures.

XRD patterns

Figure 6 shows the XRD test for graphite and nano-graphene oxide. We notice a sharp, intense peak at ~26° 2θ. This peak is characteristic of graphite (d-spacing ≈ 0.34 nm) and represents the (002) plane in the graphite crystal structure, a clear indication of the regular stacking of carbon layers. There are also several additional crystalline peaks at ~44°, 54°, 77°, and 90° 2θ [35]. These small peaks could be due to intercalary planes in the graphite crystal or to minor mineral impurities in the sample. The low background and slight diffusion indicate a high purity of the sample and a well-formed crystal structure. This spectrum corresponds to pure crystalline graphite (graphite powder) before any oxidation or reduction process. The secondary peaks correspond to higher order planes in the carbon crystal [36]. In the 2nd XRD spectrum B, we notice the absence of the characteristic graphite peak (~26° 2θ), meaning the absence of a crystalline graphite structure, and the presence of a faint, broad peak at ~10° - 12° 2θ. This broad peak indicates larger interlayer spacing (d-spacing ≈ 0.8 - 0.9 nm), a characteristic feature of graphene oxide (GO) and confirms the presence of -OH/-COOH groups between the layers. Oxygen and water groups enter between the layers, increasing the distance between them [37]. The high background and broad diffusion indicate a quasi-amorphous or alternating short-range structure, similar to that of non-thermally denatured GO films. Therefore, this spectrum corresponds to nano-GO after oxidation (before any thermal reduction steps) [38]. A 2nd diffraction maximum is noticed at 2θ = 43°, indicating the short-range stacking of graphitic layers [39].

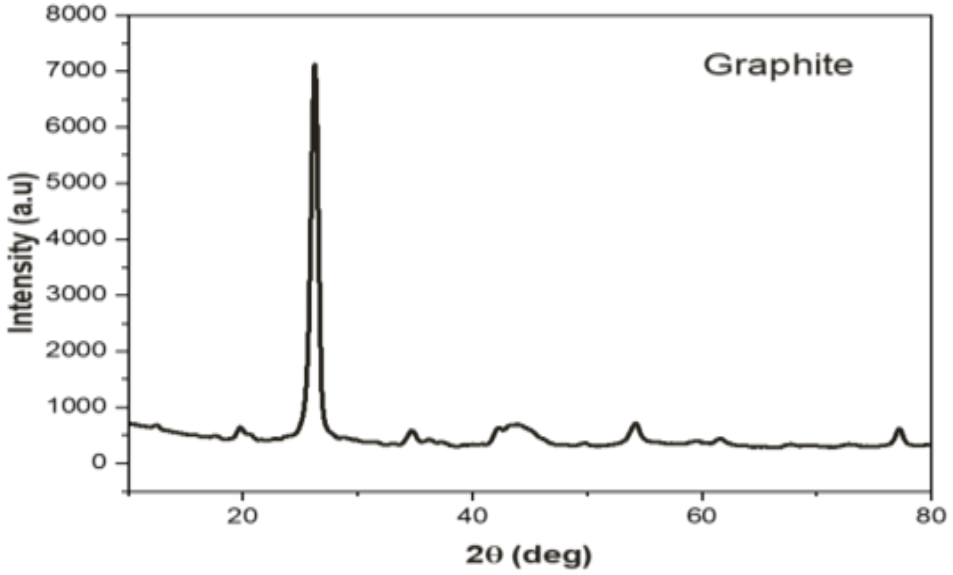

(A)

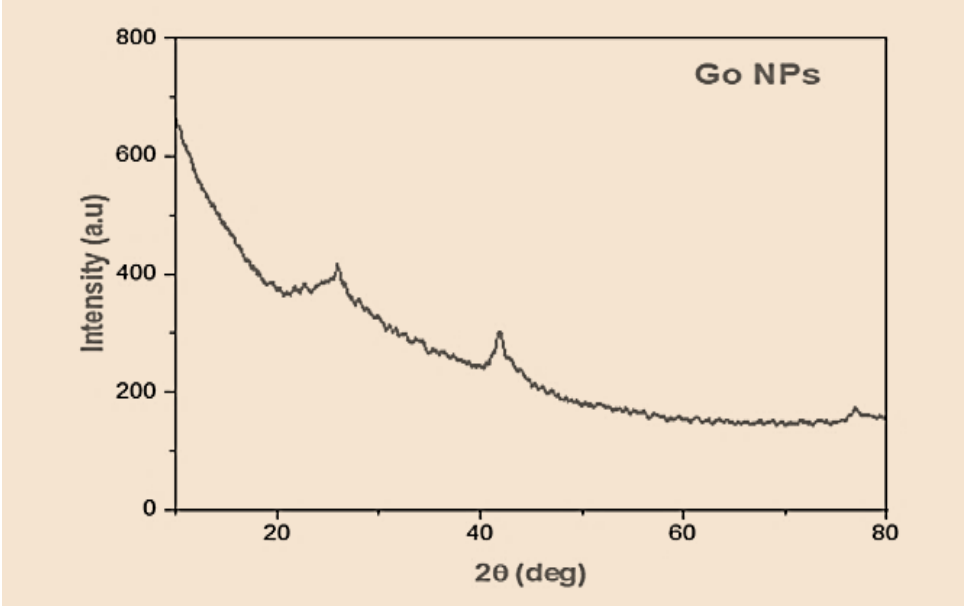

(B)

Figure 6 XRD test for (A) graphite and (B) nano graphene oxide.

Characterizations

The optical characteristics of PVA-GO nanostructures films were tested by using spectrophotometer (UV-18000A-Shimadzu). The absorption coefficient (α) is given by [40]:

$$\alpha = 2.303\ A/l \quad (1)$$

wherever: A represents the absorbance and l is the path length. One way to compute the energy gap is by [41]:

$$(\alpha h\upsilon)^{1/r} = C(h\upsilon - E_g) \quad (2)$$

where r = 2 and 3 denote permitted and prohibited indirect transitions, C is constant, hυ is the photon's energy, and E_g is the energy gap.

The extinction coefficient (k) is determined by using the following formula [42]:

$$K = \frac{a\lambda}{4\pi} \quad (3)$$

There the wavelength of the incident photon is denoted by λ. The dielectric constants (ε) is separated into 2 portions real (ε_1) and imaginary (ε_2) are computed by utilizing formulae [43]:

$$\varepsilon_1 = n^2 - k^2 \quad (4)$$

$$\varepsilon_2 = 2nk \quad (5)$$

The optical conductivity (σ_{op}) is determined by [44]:

$$\sigma_{op} = \frac{anc}{4\pi} \quad (6)$$

Optical microscopy

The distribution of GO nanoparticles within the PVA medium and the self-healing ability were examined using optical microscopy (OM) is showed **Figure 7**. All samples were measured at 40 X magnification. **Figure 7(A)** represents pure PVA without any graphene oxide additions. The surface appears largely homogeneous and almost uniform in color (closer to green in the image shown due to the lighting/lensing used) [45]. The absence of GO nanoparticles means that the surface structure is free of the agglomerations or dark spots characteristic of graphene. **Figure 7(B)** represents this sample with the highest percentage of nano-graphene oxide (0.1%) [46]. We notice more pronounced agglomerations or grains compared to the other samples, due to the higher graphene oxide concentration. The overall color tends toward yellow/dark green, which may be related to the accumulation of GO layers in certain areas. Typically, the higher the GO percentage, the greater the potential for nano-aggregates to form, which appear as spots or dark areas under the microscope. **Figure 7(C)** has a medium graphene oxide concentration (0.05%). We notice a less clumped distribution than at the 0.1% concentration, but there are still some scattered spots throughout the sample. The overall color tends toward yellowish green, perhaps less dark than the 0.1% sample because of the lower amount of GO. Overall, the surface texture will appear more homogeneous than the previous sample, but there are still visible signs of GO [47]. **Figure 7(D)** at this lower concentration (0.025%) typically shows fewer nanoclumps, or appear as scattered dark spots. The overall color becomes lighter, leaning more toward light or pale green, due to the lower amount of GO [48]. The film surface appears smoother and more homogeneous, with fewer dark spots compared to samples at higher concentrations. **Figure 7(E)** shows the lowest percentage of graphene oxide (0.012%). We observe a high degree of homogeneity in the sample, with very few dark agglomerates or spots. The color tends to be light green or even translucent, reflecting the small amount of GO distributed within the PVA Some fine dark dots may appear, but these are much fewer compared to higher concentration. Thus, we conclude that the higher the percentage of nano-graphene oxide added to the PVA, the more dark aggregates appear under the microscope, and the darker or yellower/greener the color [48]. At very low GO concentrations, the sample tends to be more homogeneous in shape and color, with very limited agglomeration. At low content, the NPs are propagated in the polymer matrix as a clusters form. With rising NPs content, the NPs shaped a network of pathways within the medium of polymer material [49-55].

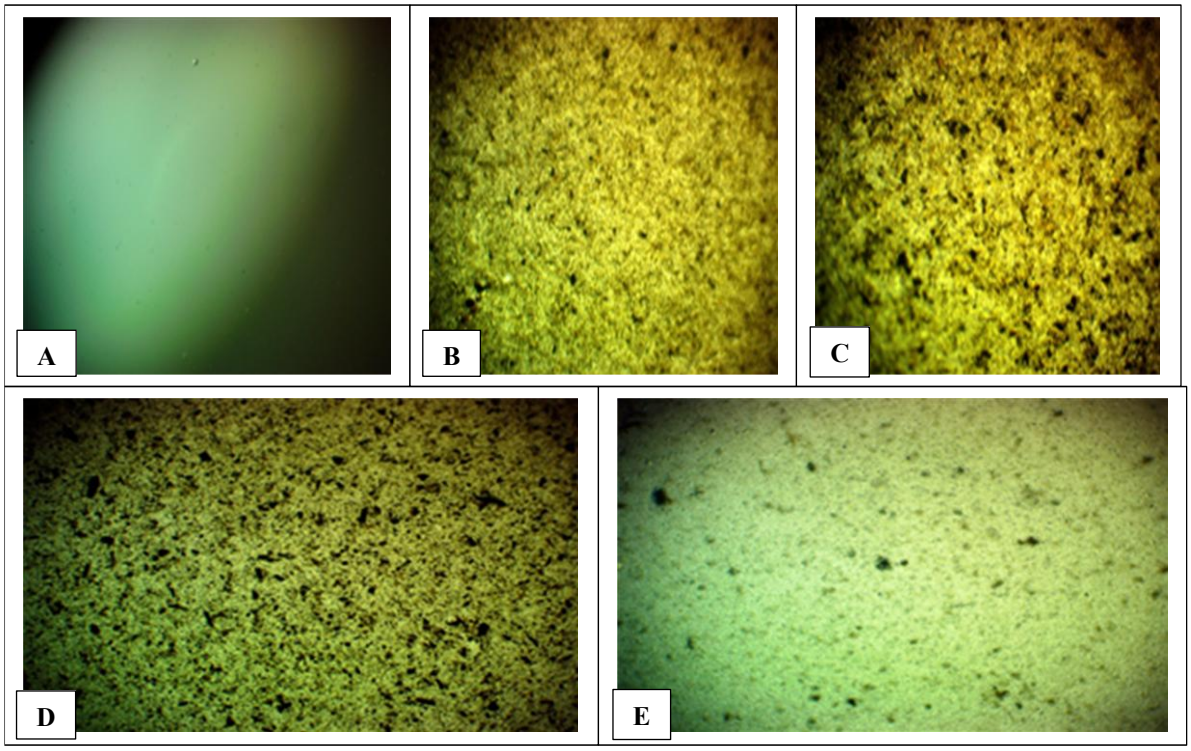

Figure 7 Optical microscopy for (PVA-GO) films: (A) pure, (B) 0.012%, (C) 0.025%, (D) 0.05%, and (E) 0.1%.

Figure 8 represents a 3D AFM (Atomic Force Microscopy) analysis of the sample surface, clearly showing changes in surface roughness before and after self-healing [56].

Figure 8(A) (roughest and highest) shows sharp, heterogeneous peaks and prominent clusters, representing the condition after damage or scratching has occurred in the material. The high roughness indicates tears or separations in the polymer network. The GO or PVA network has not yet been able to heal [56]. **Figure 8(B)** (less rough surface) shows the peaks decreasing, and the surface distribution is more uniform. This represents the initial self-healing stage, where the material begins to "fill the gaps" caused by damage by rearranging the hydrogen bonds between the GO and PVA. Self-catalyzation by moisture or heat activates the chain movements in the polymer [57].

Figure 8(C) (nearly flat surface) shows a very uniform surface distribution, with low, diffuse peaks. This represents the final condition after self-healing. The surface has been restored to almost its original state. This indicates that the GO (0.05%) ratio was ideal for efficient reaction and the polymer network was reconfigurable and gaps were closed without significant external interference. This process took half a minute at 25 °C [58].

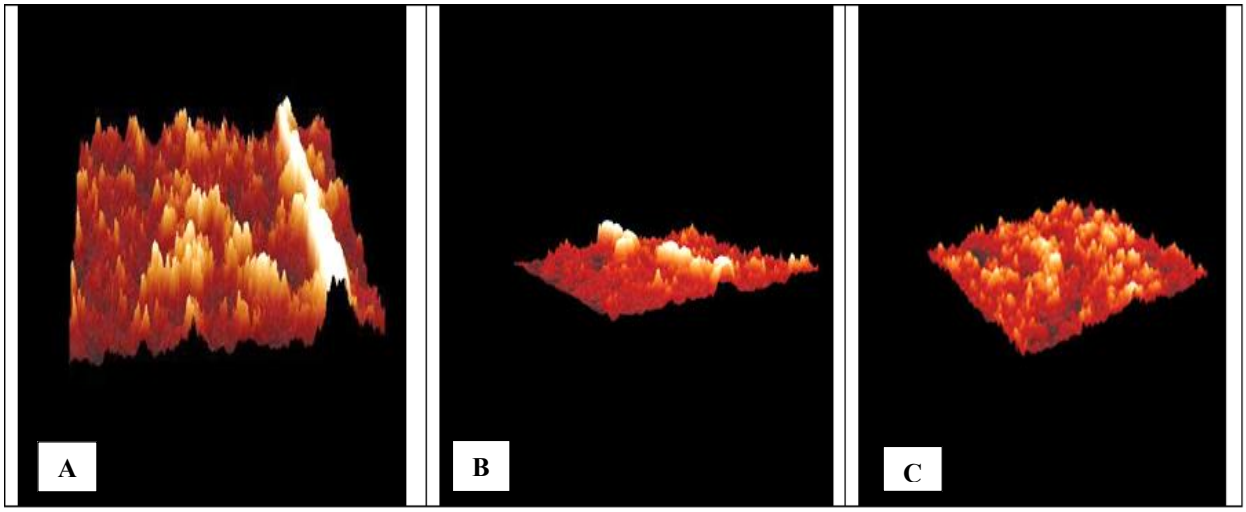

Figure 8 3D AFM (Atomic Force Microscopy) analysis of the sample surface showing changes in surface roughness before (A) and after self-healing (B), and (C) half a minute at 25 °C.

Figure 9 shows the optical microscope measurement. **Figure 9(A)** shows a polymer sample after it has been intentionally scratched or cut and subsequently undergoes self-healing. Dark and light areas can be seen in clear contrast, with the brightest areas (yellow/orange) representing areas where the polymer structure has been cut, while darker areas may indicate areas not affected [59].

Figure 9(B) the polymer begins to fill the void or crack created by the scratch. The golden/yellow color may indicate areas partially healed by the self-healing mechanism. The surface morphology shows uneven distribution of the restorative material; some areas appear relatively homogeneous, while others appear lumpy or uneven in thickness, which may reflect different stages of the self-healing process or its incompleteness. **Figure 9(C)** demonstrates the success of the self-healing process, with the scratch edges merging and a large portion of the boundaries between the crack areas disappearing. The brighter colored areas often indicate the occurrence of re-cohesion or re-formation of the chemical bonds (covalent/non-covalent bonds) responsible for the repair process. The concentration of the nanomaterial (graphene oxide) played a role in the repair mechanism, as its distribution and homogeneity affect the repair efficiency. Therefore, these images demonstrate the relative success of the self-healing mechanism of the polymer sample; the contrasting color and the disappearance of parts of the scratch indicate the initiation or completion of the repair process in a relatively record time [59,60].

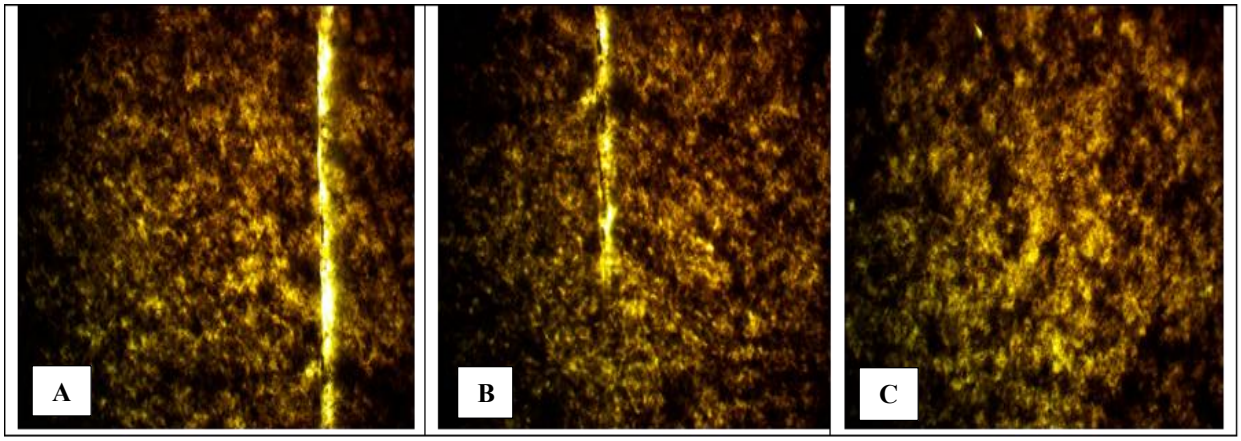

Figure 9 Optical microscope measurement for (A) scratch area, (B) partial healing, and (C) complete healing.

UV-visible radiation measurement

Figure 10 shows the UV-Vis absorption spectrum of a polyvinyl alcohol (PVA) sample incorporated with different ratios of nano-graphene oxide (GO). The spectrum ranges from 220 to 1020 nm. High absorption at lower wavelengths (220 - 300 nm). All samples exhibit high absorption in this region, which is common due to the presence of π - π* bonds in GO, especially in unsaturated C=C bonds. The higher the GO ratio (from 0.012 to 0.1) [58]. The higher absorption across the entire spectrum. This indicates that GO contributes significantly to the improvement of light absorption due to the presence of oxidized functional groups and the large surface area of graphene and rising the charges carriers numbers inside nanocomposites. The sample containing 0.1% GO exhibits the highest absorption, meaning that graphene has a strong light absorption effect, especially in the UV range. The pure PVA sample exhibits the lowest absorption, indicating that PVA does not contain many UV- and V-absorbing groups and therefore incorporates GO within PVA significantly improves absorption [60-66]. The spectrum indicates that there is good interaction and integration between GO and PVA. The regular and gradient spectrum with increasing GO concentration indicates a homogeneous distribution of GO within the polymer matrix, which means that the properties of the artificial leather (such as mechanical or sensory) will be uniform across the surface [58].

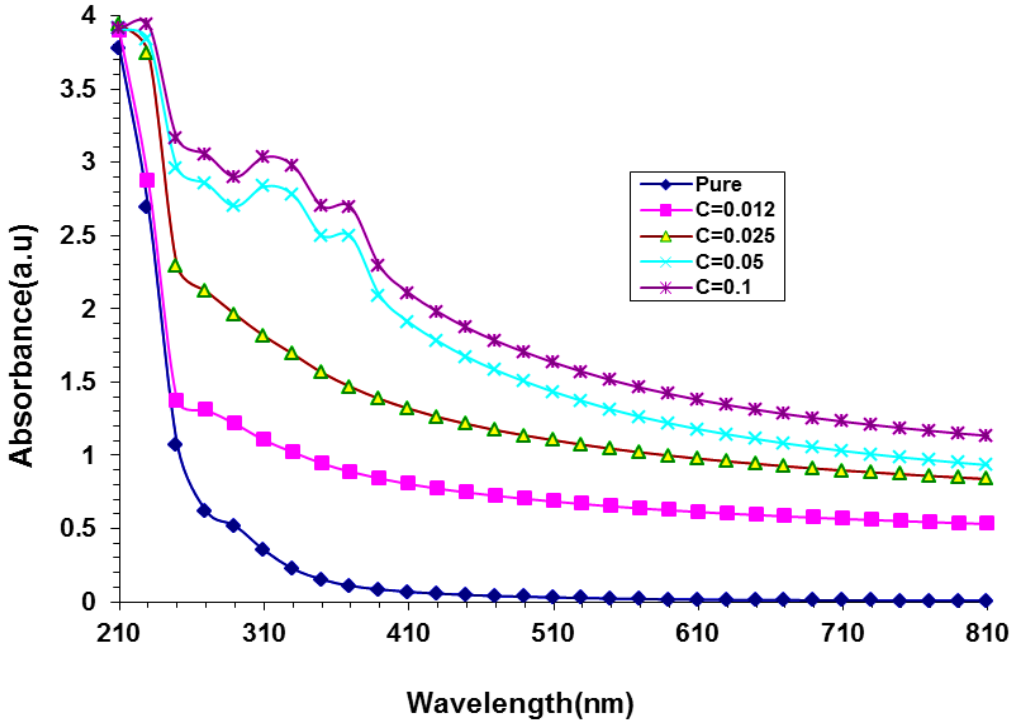

Figure 10 Variation of absorption spectrum for PVA-GO films with wavelength.

Figure 11 illustrates the effect of graphene oxide (GO) addition on the light transmittance of a given material in the spectrum from 220 to 1100 nm. The results show that increasing the GO concentration results in a decrease in transmittance, especially at short wavelengths, due to the high light absorption capacity of NPs related to increase of charges carriers [59,67-70]. Controlling optical transmittance is important in the process of preparing artificial skin. GO also contributes to mimicking the function of natural skin in protecting against harmful rays, making it a useful component in the development of smart artificial skin [56].

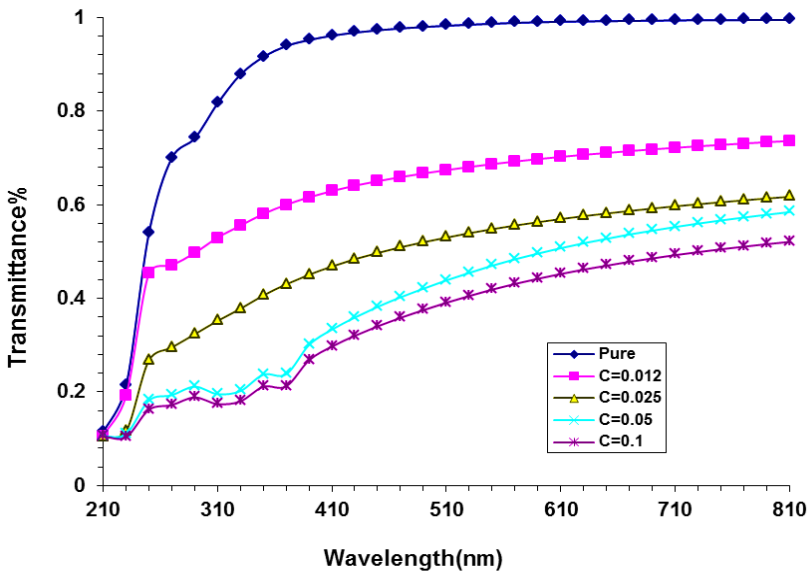

Figure 11 Effect of adding nano-graphene oxide on transmittance for PVA.

Figure 13 shows the behavior of extinction coefficient (k) for PVA-GO films with wavelength. The increasing of graphene oxide concentration leads to increase in the (k) values due to enhance the absorption [71,72]. This is useful for radiation shielding or photoreactive applications and can be exploited to tune the performance of the artificial skin as needed [73].

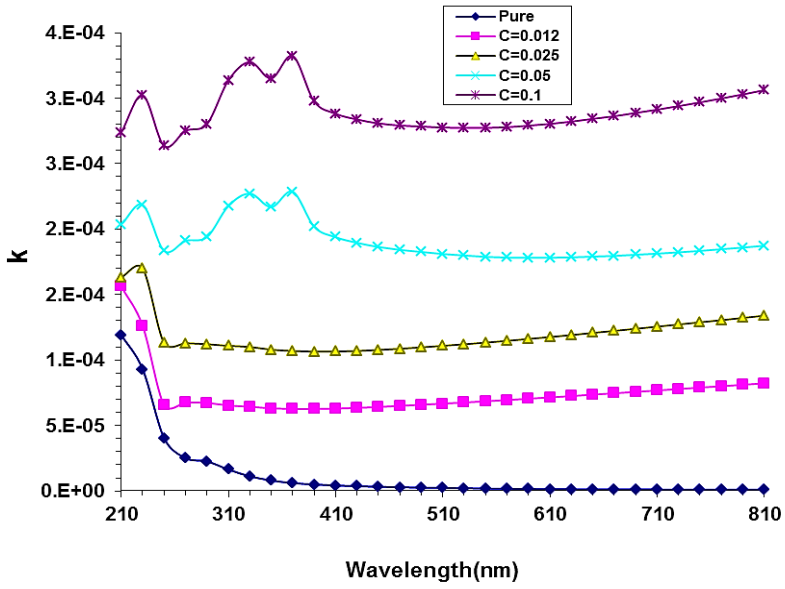

Figure 13 Behavior of extinction coefficient (k) for PVA-GO films with wavelength.

Figure 14 represents the variation of real dielectric constant for PVA-GO films with photon wavelength. It is observed that ε_1 increases significantly with increasing GO concentration, with the sample with a 0.1% GO concentration showing the highest absorption value compared to the pure sample, and rising the density of film [74,77]. This behavior indicates that the incorporation of NPs into the polymer matrix significantly enhances the material's absorbance in the ultraviolet and visible regions. This is attributed to the electronic structure of graphene oxide and its high ability to absorb light due to its presence of oxidized functional groups and localized energy states [78,79]. A gradient in values is also observed with

increasing GO concentration, supporting the hypothesis that the optical properties of the material can be controlled by adjusting the GO ratios, which is promising for artificial skin and flexible electronics applications that require tunable optical response.

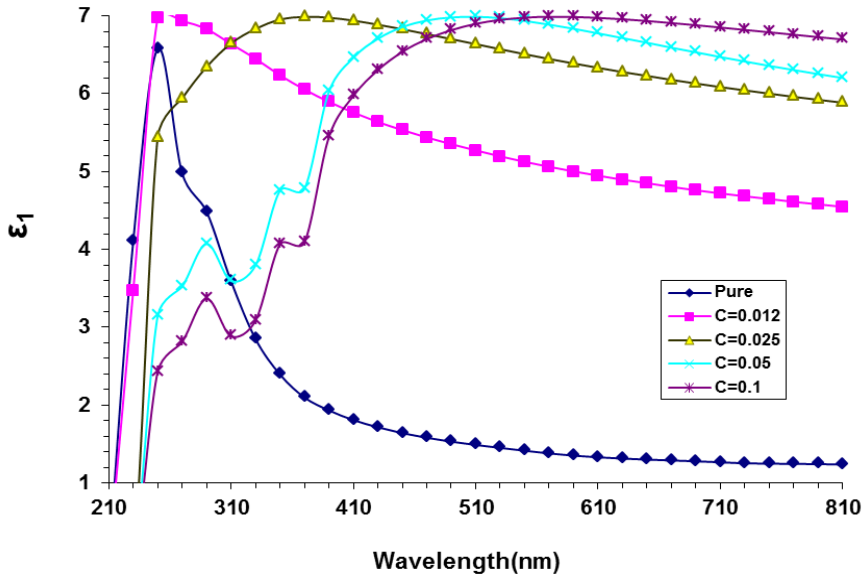

Figure 14 Variation of real dielectric constant for PVA-GO films with photon wavelength.

Figure 15 represents the imaginary dielectric constant behavior versus wavelength for PVA-GO films. The pure sample shows a significant decrease in ε_2 with increasing wavelength, indicating weak optical absorption. By adding GO, the ε_2 value increases and becomes more stable. The increase in ε_2 upon adding GO means improved optical absorption [80,81], which is useful in artificial leather to mimic the optical and thermal properties of natural skin, such as UV protection and sensitive response to light and heat.

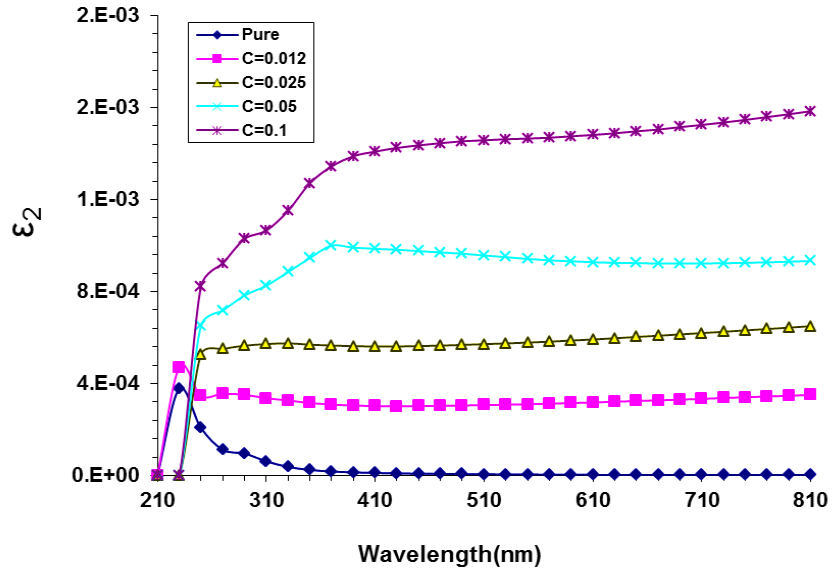

Figure 15 Imaginary dielectric constant behavior versus wavelength for PVA-GO films.

Figure 16 shows the energy gap values for PVA-GO films. The energy gap of PVA reduces with rising of GO NPs. This shift means that the indirect energy gap (E_g) decreases—from about 4.4 eV in the pure hydrogel to about 2.4 eV at 0.10 wt% GO loading—due to the GO layers introducing new electronic states into the PVA band [82,83]. This decrease allows the hydrogel to absorb a wider spectrum of visible and infrared light, generating a photothermal effect that can be exploited to activate self-healing. It also enhances the conductivity necessary for sensing pressure or temperature. In this way, it becomes possible to fine-tune the properties of artificial skin—photoprotection, electrosensitivity, and thermal activation—simply by adjusting the GO content in the hydrogel [84].

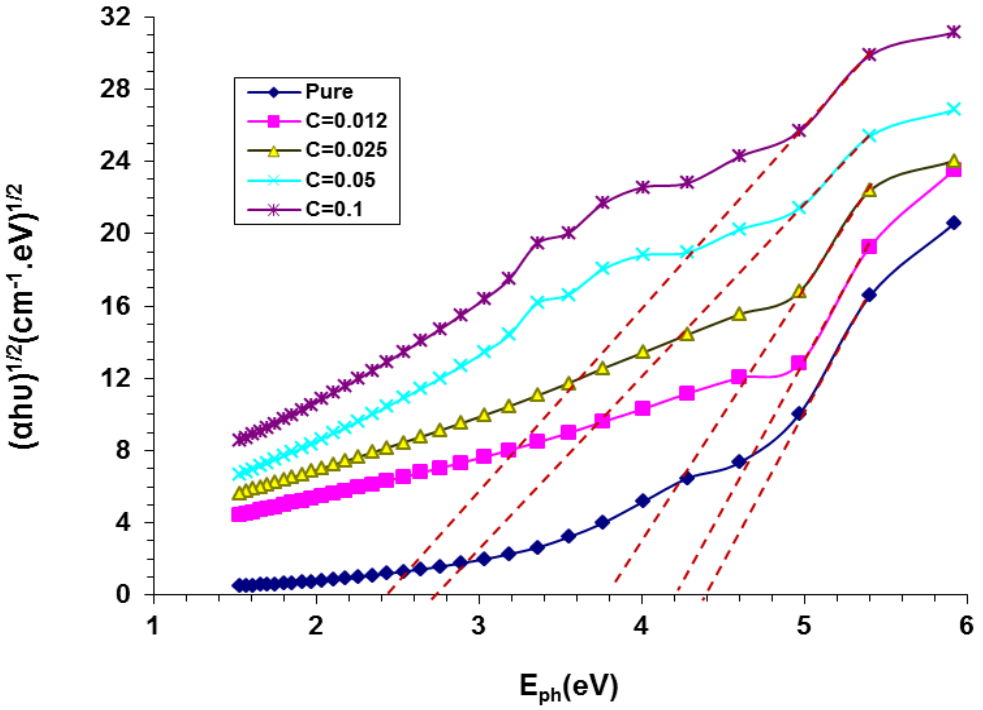

Figure 16 The indirect energy gap for (PVA-GO) nanostructures.

Conclusions

In the present work, fabrication of PVA-GO bionanocomposites films was investigated. The structural, morphological, and optical properties of PVA-GO bionanocomposites films were studied. Results established that the PVA absorbance was augment at UV/spectra when rising the GO NPs content make of 0.1 wt.%, these performances make the PVA-GO films are considerable and promising for nanoelectronics and biomedical applications. The indirect allowed energy gap reduced from 4.4 to 2.4 eV with growing content of GO NPs to 0.1 wt.%. The optical factors of PVA were improved with growing GO NPs content. Finally, the attained results showed the PVA-GO bionanocomposites films are promising nanostructures for biomedical and nanoelectronics applications.

Acknowledgments

Acknowledgment to the University of Babylon, Iraq.

CRediT Author Statement

Saja Mohammed Hussein Ali, Bahaa H. Rabee, Najah M. L. Al Maimuri, Ahmed Hashim: Wrote the main manuscript text, prepared figures and reviewed the manuscript.

References

[1] DR Dreyer, S Park, CW Bielawski and RS Ruoff. The chemistry of graphene oxide. *Chemical Society Reviews* 2010; **39(1)**, 228-240.

[2] DC Marcano, DV Kosynkin, JM Berlin, A Sinitskii, Z Sun, A Slesarev, LB Alemany, W Lu and JM Tour. Improved synthesis of graphene oxide. *ACS Nano* 2010; **4(8)**, 4806-4814.

[3] A Jiříčková, O Jankovský, Z Sofer and D Sedmidubský. Synthesis and applications of graphene oxide. *Materials* 2022; **15(3)**, 920.

[4] CI Idumah. Recent trends in MXene polymeric hydrogel bionanoarchitectures and applications. *Cleaner Materials* 2022; **5**, 100103.

[5] J Zhang, Y Qin, OJ Pambos, J Zhang, S Chen, Z Yu and C Abell. Microdroplets confined assembly of opal composites in dynamic borate ester-based networks. *Chemical Engineering Journal* 2021; **426**, 127581.

[6] M Wang, J Bai, K Shao, W Tang, X Zhao, D Lin, S Huang, C Chen, Z Ding and J Ye. Poly(vinyl alcohol) hydrogels: The old and new functional materials. *International Journal of Polymer Science* 2021; **2021**, 2225426.

[7] S Pei and HM Cheng. The reduction of graphene oxide. *Carbon* 2012; **50(9)**, 3210-3228.

[8] X Hu, R Liang, J Li, Z Liu and G Sun. Highly stretchable self-healing nanocomposite hydrogel reinforced by 5 nm particles. *ES Materials and Manufacturing* 2018; **2**, 16-23.

[9] C Lin, D Sheng, X Liu, S Xu, F Ji, L Dong, Y Zhou and Y Yang. A self-healable nanocomposite based on dual-crosslinked Graphene Oxide/Polyurethane. *Polymer* 2017; **127**, 241-250.

[10] E Zhang, T Wang, L Zhao, W Sun, X Liu and Z Tong. Fast self-healing of graphene oxide-hectorite clay-poly (N, N-dimethylacrylamide) hybrid hydrogels realized by near-infrared irradiation. *ACS Applied Materials and Interfaces* 2014; **6(24)**, 22855-22861.

[11] MO Ansari, K Gauthaman, A Essa, SA Bencherif and A Memic. Graphene and graphene-based materials in biomedical applications. *Current Medicinal Chemistry* 2019; **26(38)**, 6834-6850.

[12] PK Jha, W Khongnakorn, C Chawenjkigwanich, MS Chowdhury and K Techato. Eco-friendly reduced graphene oxide nanofilter preparation and application for iron removal. *Separations* 2021; **8(5)**, 68.

[13] PK Jha, C Chawengkijwanich, K Techato, W Limbut and M Luengchavanon. *Callistemon viminalis* leaf extract mediated biosynthesis of Ag, rGO-Ag-ZnO nanomaterials for catalytic PEM fuel cell application. *Trends in Sciences* 2022; **19(11)**, 493.

[14] PK Jha, T Jaidumrong, D Rokaya and C Ovatlarnporn. *Callistemon viminalis* leaf extract phytochemicals modified silver-ruthenium bimetallic zinc oxide nanocomposite biosynthesis: Application on nanocoating photocatalytic *Escherichia coli* disinfection. *RSC Advances* 2024; **14**, 11017.

[15] PK Jha, C Chawengkijwanich, C Pokum, P Soison and K Techato. Antibacterial activities of biosynthesized zinc oxide nanoparticles and silver-zinc oxide nanocomposites using camellia sinensis leaf extract. *Trends in Sciences* 2023; **20(3)**, 5649.

[16] A Rhazouani, H Gamrani, ME Achaby, K Aziz, L Gebrati, MS Uddin and F Aziz. Synthesis and toxicity of graphene oxide nanoparticles: A literature review of *in vitro* and *in vivo* studies. *BioMed Research International* 2021; **2021**, 5518999.

[17] S Yadav, APS Raman, H Meena, AG Goswami, Bhawna, V Kumar, P Jain, G Kumar, M Sagar, DK Rana, I Bahadur and P Singh. An update on graphene oxide: Applications and toxicity. *ACS Omega* 2022; **7(40)**, 35387-35445.

[18] PP Brisebois and M Siaj. Harvesting graphene oxide - years 1859 to 2019: A review of its structure, synthesis, properties and exfoliation. *Journal of Materials Chemistry C* 2020; **8(5)**, 1517-1547.

[19] D Chen, H Feng and J Li. Graphene oxide: Preparation, functionalization, and electrochemical applications. *Chemical Reviews* 2012; **112(11)**, 6027-6053.

[20] SMH Ali, MMM Alali and LM Ahmed. Hybrid Phosphotungstic acid-Dopamine (PTA-DA) like-flower nanostructure synthesis as a furosemide drug delivery system and kinetic study of drug

releasing. *Egyptian Journal of Chemistry* 2021; **64(10)**, 5547-5553.

[21] L Zhang, Z Wang, C Xu, Y Li, J Gao, W Wang and Y Liu. High strength graphene oxide/polyvinyl alcohol composite hydrogels. *Journal of Materials Chemistry* 2011; **21(28)**, 10399-10406.

[22] X Zhao, Q Zhang, D Chen and P Lu. Enhanced mechanical properties of graphene-based poly(vinyl alcohol) composites. *Macromolecules* 2010; **43(5)**, 2357-2363.

[23] T Cheng-an, Z Hao, W Fang, Z Hui, Z Xiaorong and W Jianfang. Mechanical properties of graphene oxide/polyvinyl alcohol composite film. *Polymers and Polymer Composites* 2017; **25(1)**, 11-16.

[24] J Cao, X Zhao and L Ye. Super-strong and anti-tearing poly (vinyl alcohol)/graphene oxide nano-composite hydrogels fabricated by formation of multiple crosslinking bonding network structure. *Journal of Industrial and Engineering Chemistry* 2022; **112**, 366-378.

[25] S Tang, Z Liu and X Xiang. Graphene oxide composite hydrogels for wearable devices. *Carbon Letters* 2022; **32(6)**, 1395-1410.

[26] H Zhang, P Ren, F Yang, J Chen, C Wang, Y Zhou and J Fu. Biomimetic epidermal sensors assembled from polydopamine-modified reduced graphene oxide/polyvinyl alcohol hydrogels for the real-time monitoring of human motions. *Journal of Materials Chemistry B* 2020; **8(46)**, 10549-10558.

[27] Y Yu, X Zhao and L Ye. A novel biocompatible wearable sensors based on poly (vinyl alcohol)/graphene oxide hydrogel with superior self-adhesion, flexibility and sensitivity. *Composite Structures* 2023; **309**, 116768.

[28] SMH Ali, MMMA Alali and LM Ahmed. Flower-like hierarchical nanostructures synthesis of polyoxometalate-dopamine and loading furosemide on its surface and aging them using microwave technique. *AIP Conference Proceedings* 2022; **2547**, 40010.

[29] A Lerf, H He, M Forster and J Klinowski. Structure of graphite oxide revisited. *The Journal of Physical Chemistry B* 1998; **102(23)**, 4477-4482.

[30] H Ahmed, A Hashim and HM Abduljalil. Analysis of Optical, Electronic and Spectroscopic properties of (Biopolymer-SiC) Nanocomposites for Electronics Applications. *Egyptian Journal of Chemistry* 2019; **62(9)**, 1659-1672.

[31] A Hashim, MA Habeeb, A Khalaf and A Hadi. Fabrication of (PVA-PAA) Blend-Extracts of Plants Bio-Composites and Studying Their Structural, Electrical and Optical Properties for Humidity Sensors Applications. *Sensor Letters* 2017; **15**, 589-596.

[32] G Eda and M Chhowalla. Chemically derived graphene oxide: Towards large-area thin-film electronics and optoelectronics. *Advanced Materials* 2010; **22(22)**, 2392-2415.

[33] X Huang, X Qi, F Boey and H Zhang. Graphene-based composites. *Chemical Society Reviews* 2012; **41(2)**, 666-686.

[34] ZWK Low, Z Li, C Owh, PL Chee, E Ye, K Dan, SY Chan, DJ Young and XJ Loh. Recent innovations in artificial skin. *Biomaterials Science* 2020; **8(3)**, 776-797.

[35] V Kammarchedu, H Asgharian, K Zhou, PS Khamsi and A Ebrahimi. Recent advances in graphene-based electroanalytical devices for healthcare applications. *Nanoscale* 2024; **16**, 12857-12882.

[36] H Chen, F Zhuo, J Zhou, Y Liu, J Zhang, S Dong, X liu, A Elmarakbi, H Duan and Y Fu. Advances in graphene-based flexible and wearable strain sensors. *Chemical Engineering Journal* 2023; **464**, 142576.

[37] J Tavakoli and Y Tang. Hydrogel based sensors for biomedical applications: An updated review. *Polymers* 2017; **9(8)**, 364.

[38] Y Gao, X Wang and C Fan. Advances in graphene-based 2D materials for tendon, nerve, bone/cartilage regeneration and biomedicine. *iScience* 2024; **27(7)**, 110214.

[39] S Constantinescu, AG Niculescu, A Hudiță, V Grumezescu, D Rădulescu, AC Bîrcă, G Dorcioman, O Gherasim, AM Holban, B Gălățeanu, BS Vasile, AM Grumezescu, A Bolocan and R Rădulescu. Nanostructured coatings based on graphene oxide for the

management of periprosthetic infections. *International Journal of Molecular Sciences* 2024; **25**, 2389.

[40] OC Compton and ST Nguyen. Graphene oxide, highly reduced graphene oxide, and graphene: Versatile building blocks for carbon-based materials. *Small* 2010; **6(6)**, 711-723.

[41] AMA Henaish and AS Abouhaswa. Effect of WO3 nanoparticle doping on the physical properties of PVC polymer. *Bulletin of Materials Science* 2020; **43**, 149.

[42] N Mahfoudh, K Karoui and AB Rhaiem. Optical studies and dielectric response of $[DMA]_2MCl_4$ (M = Zn and Co) and $[DMA]_2ZnBr_4$. *RSC Advances* 2021; **11(40)**, 24526-24535.

[43] A Alsaad, ARA Dairy, A Ahmad, IA Qattan, SA Fawares and Q Al-Bataineh. Synthesis and Characterization of Polymeric (PMMA-PVA) hybrid thin films doped with TiO2 nanoparticles using dip-coating technique. *Crystals* 2021; **11(2)**, 99.

[44] AO Salohub, AA Voznyi, OV Klymov, NV Safryuk, DI Kurbatov and AS Opanasyuk. Determination of fundamental optical constants of Zn_2SnO_4 films. *Semiconductor Physics, Quantum Electronics and Optoelectronics* 2017; **20(1)**, 79-84.

[45] MK Mohammed, MH Abbas, A Hashim, BH Rabee, MA Habeeb and N Hamid. Enhancement of optical parameters for PVA/PEG/Cr_2O_3 nanocomposites for photonics fields. *Journal of Composite and Advanced Materials* 2022; **32(4)**, 205-209.

[46] S Stankovich, DA Dikin, GHB Dommett, KM Kohlhaas, EJ Zimney, EA Stach, RD Piner, ST Nguyen and RS Ruoff. Graphene-based composite materials. *Nature* 2006; **442(7100)**, 282-286.

[47] S Park and RS Ruoff. Chemical methods for the production of graphenes. *Nature Nanotechnology* 2009; **4(4)**, 217-224.

[48] S Park and RS Ruoff. Erratum: Chemical methods for the production of graphenes. *Nature Nanotechnology* 2010; **5**, 309.

[49] HAJ Hussien and A Hashim. Fabrication and analysis of PVA/TiC/SiC hybrid nanostructures for nanoelectronics and optics applications. *Journal of Inorganic and Organometallic Polymers and Materials* 2024; **34(6)**, 2716-2727.

[50] HK Jaafar, A Hashim and BH Rabee. Fabrication and unraveling the morphological, structural, and dielectric features of PMMA-PEO-SiC-$BaTiO_3$ promising quaternary nanocomposites for multifunctional nanoelectronics applications. *Journal of Materials Science: Materials in Electronics* 2024; **35**, 128.

[51] A Kareem, A Hashim and HB Hassan. Ameliorating and tailoring the morphological, structural, and dielectric features of Si_3N_4/CeO_2 futuristic nanocomposites doped PEO for nanoelectronic and nanodielectric applications. *Journal of Materials Science: Materials in Electronics* 2024; **35**, 461.

[52] HK Jaafar, A Hashim and BH Rabee. Tailoring the influence of hybrid SiC/$SrTiO_3$ nanomaterials doped PMMA/PEO for promising nanodielectric and nanoelectronic applications. *Silicon* 2024; **16**, 1905-1915.

[53] MH Abbas, H Ibrahim, A Hashim and A Hadi. Fabrication and tailoring structural, optical, and dielectric properties of PS/$CoFe_2O_4$ nanocomposites films for nanoelectronics and optics applications. *Transactions on Electrical and Electronic Materials* 2024; **25**, 449-457.

[54] Z Sattar and A Hashim. Synthesis of PMMA/PEG/SiO_2/SiC multifunctional nanostructures and exploring the microstructure and dielectric features for flexible nanodielectric applications. *Silicon* 2024; **16(17)**, 6181-6192.

[55] Z Sattar and A Hashim. Quaternary PMMA-PEG/SnO_2-SiC nanocomposite films for flexible nanodielectric and energy storage applications. *Silicon* 2025; **17**, 1681-1692.

[56] Y Zhu, S Murali, W Cai, X Li, JW Suk, JR Potts and RS Ruoff. Graphene and graphene oxide: Synthesis, properties, and applications. *Advanced Materials* 2010; **22(35)**, 3906-3924.

[57] W Choi, I Lahiri, R Seelaboyina and YS Kang. Synthesis of graphene and its applications: A review. *Critical Reviews in Solid State and Materials Sciences* 2010; **35(1)**, 52-71.

[58] S Ryu, L Liu, S Berciaud, YJ Yu, H Liu, P Kim, GW Flynn and LE Brus. Atmospheric oxygen binding and hole doping in deformed graphene on

a SiO2 substrate. *Nano Letters* 2010; **10(12)**, 4944-4951.

[59] S Johari, MM Ramli, MF Ahmad, NH Osman and AH Reshak. *Analytical tools for characterizing*. *In*: Hybrid-nanomaterials. Springer, Singapore, 2024, p. 23-38.

[60] J Yang. 2016, Phosphonium ionic liquids: Versatile nanostructuration and interfacial agents for poly (vinylidene fluoride-chlorotrifluoroethylene). Ph. D. Dissertation. Université de Lyon, Lyon, France.

[61] A Hashim, FL Rashid, MH Abbas and BH Rabee. Preparation of nanofluids from inorganic nanostructures doped PEG: Characteristics and energy storage applications. *East European Journal of Physics* 2023; **1**, 185-188.

[62] A Hashim, SM Alshrefi, HH Abed and A Hadi. Synthesis and boosting the structural and optical characteristics of PMMA/SiC/CdS hybrid nanomaterials for future optical and nanoelectronics applications. *Journal of Inorganic and Organometallic Polymers and Materials* 2024; **34**, 703-711.

[63] A Hashim, B Mohammed, A Hadi and H Ibrahim. Synthesis and augment structural and optical characteristics of PVA/SiO_2/$BaTiO_3$ nanostructures films for futuristic optical and nanoelectronics applications. *Journal of Inorganic and Organometallic Polymers and Materials* 2024; **34**, 611-621.

[64] A Hashim, A Hadi and MH Abbas. Synthesis and unraveling the morphological and optical features of PVP-Si_3N_4-Al_2O_3 nanostructures for optical and renewable energies fields. *Silicon* 203; **15**, 6431-6438.

[65] H Ahmed and A Hashim. Design and tailoring the structural and spectroscopic characteristics of Sb_2S_3 nanostructures doped PMMA for flexible nanoelectronics and optical fields. *Optical and Quantum Electronics* 2023; **55(3)**, 280.

[66] HK Jaafar, A Hashim and BH Rabee. Fabrication and tuning the morphological and optical characteristics of PMMA/PEO/SiC/$BaTiO_3$ newly quaternary nanostructures for optical and quantum electronics fields. *Optical and Quantum Electronics* 2023; **55(11)**, 989.

[67] HAJ Hussien, RG Kadhim and A Hashim. Investigating the low cost photodegradation performance against organic pollutants using CeO_2/MnO_2/ polymer blend nanostructures. *Optical and Quantum Electronics* 2022; **54**, 704.

[68] HAJ Hussien, RG Kadhim and A Hashim. Tuning the optical characteristics of SiO_2/MnO_2 nanostructures doped organic blend for photodegradation of organic dyes. *Optical and Quantum Electronics* 2021; **53**, 501.

[69] HB Hassan, A Hashim and HM Abduljalil. Tailoring structural, optical characteristics of CuO/In_2O_3 nanoparticles-doped organic material for photodegradation of dyes pollutants. *Polymer Bulletin* 2023; **80**, 9059-9075.

[70] A Kareem, A Hashim and HB Hassan. Synthesis and boosting the morphological, structural and optical features of PEO/Si_3N_4/CeO_2 promising nanocomposites films for futuristic nanoelectronics applications. *Silicon* 2024; **16(7)**, 2827-2838.

[71] A Hashim, A Hadi, H Ibrahim and FL Rashid. Fabrication and boosting the morphological and optical properties of PVP/SiC/Ti nanosystems for tailored renewable energies and nanoelectronics fields. *Journal of Inorganic and Organometallic Polymers and Materials* 2024; **34**, 1678-1688.

[72] HK Jaafar, A Hashim and BH Rabee. Synthesis and boosting the morphological and optical characteristics of SiC/$SrTiO_3$ nanomaterials doped PMMA/PEO for tailored optoelectronics fields. *Silicon* 2024; **16**, 603-614.

[73] AKK Padinjareveetil, VVT Padil and M Černík. *Graphene oxide-based nanocomposite and their biomedical applications*. *In*: S Jana and S Jana (Eds.). Nanoengineering of biomaterials. John Wiley & Sons, New Jersey, 2022, p. 427-456.

[74] FA Jasim, A Hashim, AG Hadi, F Lafta, SR Salman and H Ahmed. Preparation of (pomegranate peel-polystyrene) composites and study their optical properties. *Research Journal of Applied Sciences* 2013; **8(9)**, 439-441.

[75] HB Hassan, A Hashim and HM Abduljalil. Synthesis, structural and optical characteristics of PEO/NiO/In_2O_3 hybrid nanomaterials for

photodegradation of pollutants from wastewater. *Optical and Quantum Electronics* 2023; **55**, 556.

[76] A Hashim, H Ibrahim and A Hadi. Fabrication and augmentation of optical and structural characteristics of PVA/SiC/$CoFe_2O_4$ hybrid nanocomposites for tailored optical and quantum electronics applications. *Optical and Quantum Electronics* 2024; **56**, 1177.

[77] A Hashim, HH Abed and SM Alshrefi. Ameliorating and tuning the structural, morphological, and optical characteristics of chromium oxide/silicon carbide promising hybrid nanocomposites doped PMMA for futuristic nanoelectronics and photonics applications. *Silicon* 2024; **16**, 5087-5095.

[78] G Ahmed, AF Kadhim, A Hashim and H Ibrahim. Fabrication and exploring the structural and optical features of Si_3N_4/SiO_2 hybrid nanomaterials doped PMMA for promising optoelectronics fields. *Optical and Quantum Electronics* 2024; **56**, 1308.

[79] AF Kadhim, G Ahmed and A Hashim. Fabrication and tuning the structural and optical features of SiO_2/Si_3N_4 nanomaterials doped PS for promising optoelectronics applications. *Journal of Inorganic and Organometallic Polymers and Materials* 2024; **34**, 4267-4276.

[80] FA Jasim, F Lafta, A Hashim, M Ali and AG Hadi. Characterization of palm fronds-polystyrene composites. *Journal of Engineering and Applied Sciences* 2013; **8(5)**, 140-142.

[81] S Hadi, A Hashim and A Jewad. Optical properties of (PVA-LiF) composites. *Australian Journal of Basic and Applied Sciences* 2011; **5(9)**, 2192-2195.

[82] WO Obaid, A Hashim and BH Rabee. Manufacturing and ameliorating the morphological, structural and optical features of PVA-CS/SiO_2-TaC futuristic nanostructures for radiation shielding and photonics applications. *Journal of Inorganic and Organometallic Polymers and Materials* 2025; **35**, 10346-10359.

[83] A Hashim, A Kareem, H Ibrahim, D Uthra, A Hadi, K Thakur and JP Chandra. Fabrication and ameliorating the features of (PMMA-SiC-NiO) multifunctional nanostructures for flexible optoelectronics applications. *Journal of Inorganic and Organometallic Polymers and Materials* 2025; **35**, 8876-8888.

[84] BH Rabee and I Oreibi. Fabrication of new nanocomposites (PMMA-SPO-PS-TiC) and studying their structural and electrical properties for humidity sensors. *Bulletin of Electrical Engineering and Informatics* 2018; **7(4)**, 538-546.